

Modeling and Testing of a Bidirectional Smart Charger for Distribution System EV Integration

Mauricio Restrepo, *Student Member, IEEE*, Jordan Morris, Mehrdad Kazerani, *Senior Member, IEEE*,
Claudio A. Cañizares, *Fellow, IEEE*

Abstract—This paper proposes a model of a single-phase bidirectional electric vehicle (EV) charger with capability of operating in all four quadrants of the P-Q plane. The steady-state and step responses of the proposed model are used to validate it, based on the actual responses of a bidirectional charger prototype for different P-Q requests. The model can be used efficiently in time-domain simulations that require models of a number of EV chargers, such as EV integration studies in low-voltage (LV) distribution networks. A practical case study is presented to demonstrate and test the proposed smart charger and model, investigating the provision of vehicle-to-grid (V2G) for active and reactive power in an LV residential distribution network. These results demonstrate the advantages of the presented charger model for developing V2G strategies in distribution networks.

Index Terms—Charging control, distribution networks, electric vehicle (EV), EV charger modeling, smart battery charger, V2G.

GLOSSARY AND NOMENCLATURE

Acronyms

ADC	Analog-to-digital converter
CC	Constant current
CCU	Central control unit
CP	Constant power
CV	Constant voltage
EV	Electric vehicle
LV	Low-voltage
PHEV	Plug-in hybrid electric vehicle
PI	Proportional-integral
PLL	Phase-locked loop
PR	Proportional-resonant
PWM	Pulse width modulation
V2G	Vehicle-to-grid
VSC	Voltage source converter

Parameters

ω	Angular frequency [rad/s]
C	Capacitance [mF]
k_i	Integral gain constant
k_p	Proportional gain constant
L	Inductance [mH]
N_v	Number of EVs connected in each phase
R	Resistance [Ω]

This work was supported by an NSERC CRD and ORF grants, in collaboration with Hydro One Networks Inc. and IBM.

M. Restrepo, M. Kazerani, and C. Cañizares are with the Department of Electrical and Computer Engineering, University of Waterloo, Waterloo, ON N2L 3G1, Canada (email: mrestrep@uwaterloo.ca; mkazerani@uwaterloo.ca; ccanyzares@uwaterloo.ca)

J. Morris is with Tesla Motors, Inc.

SW	Switch
T	Period [s]

Indices

α	α -axis component in $\alpha\beta$ transform
β	β -axis component in $\alpha\beta$ transform
b	Battery
c	Coupling
d	Direct-axis
dc	Direct current
f	Filter
$meas$	Measured
mod	Modulation
oc	Open circuit
q	Quadrature-axis
ref	Reference
req	Request
s	System

Variables

θ	Angle [rad]
D	Duty cycle
i, I	Instantaneous and RMS current [A]
M	Modulation index
m	Modulation signal
P	Active Power [kW]
Q	Reactive Power [kVAR]
S	Apparent Power [kVA]
SF	Switching Function
SoC	State of Charge
v, V	Instantaneous and RMS voltage [V]

I. INTRODUCTION

IN the last two decades, plug-in and plug-in hybrid electric vehicles (EVs) have emerged as adequate alternatives to internal combustion engine vehicles to reduce greenhouse gas emissions. However, many experts have expressed concerns about the effects of mass deployment of EVs on power systems, and thus a number of studies have been carried out to analyze these impacts. Nowadays, there is a consensus among researchers that the bottleneck for EV mass deployment will be distribution systems, since beyond some relatively low penetration levels, problems such as undervoltages in system nodes and overloadings in feeders and transformers are likely [1].

To alleviate the negative impacts of EVs on distribution systems, several researchers have proposed smart charging

strategies, which consist of enforcing controlled EV charging profiles to reduce energy costs, avoiding to exceed the operative limits of power systems, and decreasing system losses [1]. One of these strategies is vehicle-to-grid (V2G), which uses the EV battery to store energy during low-consumption/low-price hours, and discharges the battery when the energy is needed [2]. This approach requires EVs to be equipped with bidirectional chargers, and various works have demonstrated the feasibility of these types of chargers, exploring several converter topologies and control strategies; in fact, Nissan has announced the release of an EV Leaf with V2G capabilities [3]. These chargers include three-level pulse width modulation (PWM) ac/dc converters based on neutral point clamped control [4], single-phase half-bridge rectifier for power quality compensation [5], or split-phase three-phase converter with protective earth at one of the legs and a proportional-resonant (PR) controller [6]. Additionally, other experimental works have been reported on bidirectional chargers that are able to operate in a wide range of power factors, thus enabling reactive power control. These papers explore various topologies and control strategies, such as PR controllers to regulate the utility line current with full bridge ac/dc converters [7], single-phase, three-wire charger with unbalanced current compensation [8], single-phase charger with power angle control [9], three-phase off-board charger with boost rectifier [10], and single-phase two-stage bidirectional EV charger for V2G reactive power operation [11].

The aforementioned works demonstrate the practical feasibility of bidirectional chargers; however, there is a need to study their voltage interactions with other chargers and loads in distribution systems, which can last from tens of milliseconds to a few seconds, depending on the dynamic characteristics of the electrical devices connected to the distribution network. Usually, the impacts of these interactions are analyzed on the primary distribution system, considering EVs as aggregated loads (e.g., [12], [13]). Furthermore, very few studies have been performed on the effects of EVs on the secondary distribution system, even though an EV charger demand can be as high as a typical household peak demand, thus impacting directly voltage levels in distribution systems, and the loadability of distribution transformers. To understand the effects of EV chargers in secondary distribution systems, and implement control strategies to mitigate those effects, it is required to model, in detail, the equipment connected to the secondary distribution network. Hence, such a model should consider switching dynamics, thus requiring small simulation time steps in order to account for the high switching frequency (that can be in the order of 20kHz), demanding time-consuming and costly computations [14]. This is impractical for distribution network types of studies which involve multiple chargers and various other equipment models.

To overcome the previously mentioned problem, average modeling has been used in power electronics. This modeling approach concentrates on converter cycle-to-cycle behavior, and neglects the switching dynamics within a switching period, improving the simulation efficiency without sacrificing the capability of predicting the converter steady-state and dynamic responses [15], thus making it a practical approach

for simulating EV chargers in distribution system studies. However, not much has been reported on EV charger average modeling. For example, in [14], an average model is proposed for a unidirectional EV charger composed of a diode bridge rectifier, a power factor corrector stage (boost converter), and a dc/dc converter, which is then used to study voltage regulation effects of EV chargers in a distribution network. On the other hand, for bidirectional chargers with single-stage topologies, average models have been reported, mainly for full-bridge ac/dc converters [16], [17]; however, these papers have focused on small-signal modeling for controller design and not for grid impact analysis. For two-stage and integrated bidirectional charger topologies, some works have proposed average models for the study of individual stages of these chargers (e.g., [18], [19]).

The objective of this paper is to describe a new average model of a single-phase, two-stage bidirectional charger, that is able to operate in all four quadrants of the P-Q plane, in order to efficiently study the interaction of several of these chargers in a practical secondary distribution system using time domain simulations, as demonstrated here. Four quadrants operation is considered here to add controllability to the distribution network through EV chargers, which are used here as reactive power sources to improve the household power factors and contribute to voltage regulation in distribution networks. Thus, the main contributions of this paper are:

- An average model of a single-phase, four-quadrant bidirectional EV charger, which can be easily integrated into time-domain simulations to analyze the impacts of this type of chargers in distribution networks, is proposed
- The proposed average model is validated with an actual bidirectional EV charger prototype.
- Three operation strategies of bidirectional EV chargers in LV distribution systems are presented and discussed, illustrating their application through time-domain simulations based on the proposed average model.

Thus, Section II presents the characteristics of the bidirectional charger that is analyzed in this paper. Then, Section III describes the formulation leading to the average model of the chosen bidirectional charger topology. In Section IV, the average model is validated by comparing its responses in steady state and dynamic conditions with those of a developed charger prototype. Section V illustrates the use of the average model to study the impact of several bidirectional chargers in a residential secondary distribution system, exploring three V2G control strategies that may be employed with such EV chargers. Finally, Section VI highlights the main conclusions and contributions of the presented work.

II. BIDIRECTIONAL CHARGER

A. Charger Topology

The bidirectional charger analyzed in this work is a Level 1 charger rated at 1.92 kVA/120 V, and has a two-stage topology. This configuration was chosen because of its popularity and simplicity [20]–[23]. Stage 1 is a full-bridge ac/dc converter, and Stage 2 is a bidirectional buck-boost dc/dc converter, as

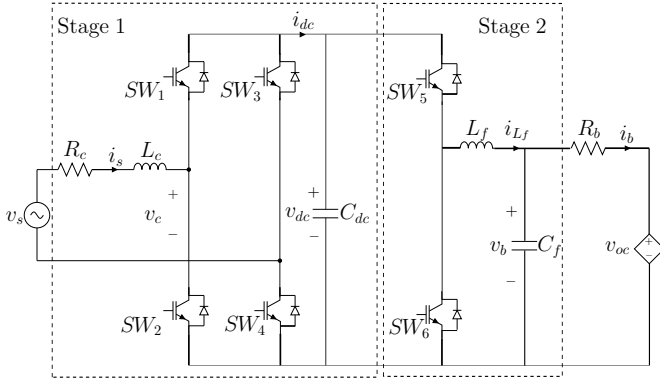


Fig. 1. Single-phase bidirectional battery charger topology.

shown in Fig. 1. The role of Stage 1 is to regulate the dc-link voltage at the desired power factor at the grid interface; the role of the Stage 2 is to control charging and discharging of the battery according to the desired active power level. This necessitates decoupling of the active and reactive power controls, with reactive power requests being processed by the ac/dc controller and active power requests being processed by the dc/dc controller. In the next subsections, the control strategy that ensures decoupled control of active and reactive power is explained. Based on the significant advantages of using a direct-quadrature (dq) controller highlighted next, this is used here as the ac/dc reactive power controller.

B. AC/DC Converter Controller

Presently, most applications of PWM voltage-source converter (PWM-VSC) use a PWM-Current-Control (PWM-CC) technique, which provides benefits such as good control of current and regulation of dc-link voltage, and compensation of semiconductor device voltage drop and switch dead time [24]. A good part of the literature available on this subject agrees that the two top choices for linear non-predictive control are the stationary frame PR controller and the synchronous frame dq controller [25]–[27].

Synchronous frame controllers are widely used in current control of three-phase voltage-source converters (VSCs), due to their ability to achieve zero steady-state error. The idea behind synchronous frame control is to transform time varying quantities, such as current and voltage, into time-invariant quantities, so that linear control can be implemented without introducing steady-state error. In three-phase systems, the most common transformation is the direct-quadrature-zero (dq0) transform, which cannot be applied directly in single-phase systems since it requires at least two signals. A common approach in single-phase systems is to apply first an $\alpha\beta$ transform by keeping the original signal as the α component, and introducing a delay of 90° over the original signal to obtain the β component; after that, the $\alpha\beta$ signals are transformed to dq components [28]. In this kind of controllers, a phase-locked loop (PLL) is needed to determine the fundamental frequency, as well as to produce an angle θ to synchronize the dq frame to the grid voltage. The block diagram for a dq-controller is given in Fig. 2 [26]. In this controller, the error term for the

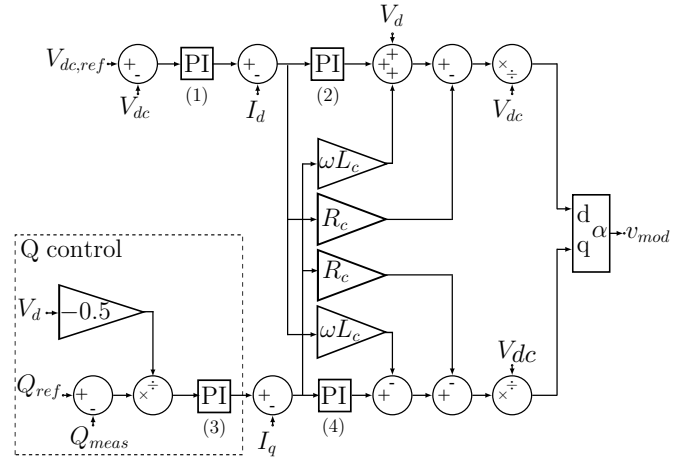


Fig. 2. AC/DC dq controller with reactive power support.

dc link voltage V_{dc} is fed through a proportional-integral (PI) regulator and then used as the reference term for I_d . The I_q reference is derived from the desired reactive power. Thus, for $V_q = 0$, due to the PLL action, one has that:

$$S = P_s + jQ_s = 0.5V_d I_d - 0.5jV_d I_q \quad (1)$$

where all variables in this and other equations and figures in the paper are defined in the Nomenclature section. The only controllable variable on the right hand side of (1) is I_q , since V_d is determined by the system voltage v_s , and I_d is determined by the battery current and losses in the system. Therefore, by setting $I_{q,ref}$, reactive power can be controlled, decoupled from active power control. To obtain this value, Q_{ref} is subtracted from Q_{meas} , then divided by $-0.5V_d$, and fed to a PI regulator to produce $I_{q,ref}$. This solution allows reactive power to be readily calculated with its control being decoupled from active power control.

The remaining part of the controller implements the relation between the system voltage v_s and the coupling voltage v_c , scaled down by V_{dc} to produce a usable value for v_{mod} . The dq- $\alpha\beta$ transform is performed on these values, resulting in v_β being discarded and $v_\alpha = v_{mod}$. Since this controller operates on time-invariant dc quantities, it is able to achieve zero-steady state error and high-quality voltage regulation, and is highly immune to disturbances [29], [30]; moreover, it inherently makes it easy to control reactive power.

C. DC/DC Converter Controller

The active power flow from/to the grid is dictated by the battery current, battery voltage, and losses in the charger. The function of the ac/dc controller is to regulate the dc link voltage, and if properly tuned, it will be able to automatically respond to changes in the dc link voltage by either pulling power from the grid, if the dc link voltage drops, or pushing power to the grid, if the dc link voltage rises. Thus, by controlling the charging and discharging of the battery with the dc/dc converter component of the charger, active power control can be achieved.

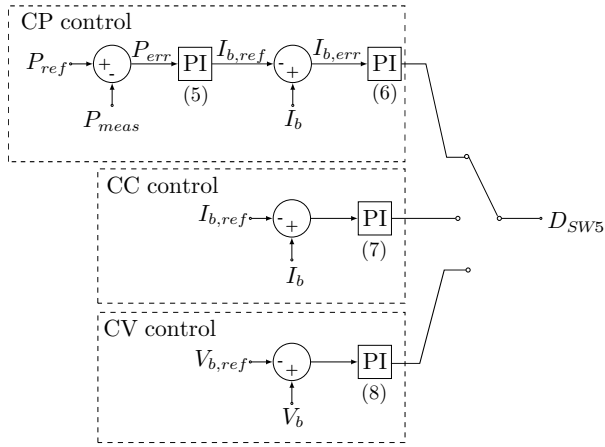


Fig. 3. DC/DC converter controller.

The proposed control uses the active power request at the grid interface (P_{ref}) sent by the utility to dictate the charging current, as shown in Fig. 3, where P_{meas} is the calculated real component from (1), representing the active power at the point of common coupling; the error is processed by a PI regulator to determine $I_{b,ref}$. This is a nested-loop control structure where the outer loop has a slower response than the inner loop. This controller is also able to perform constant current (CC)-constant voltage (CV) charging, as it is normally done with lithium-ion batteries, which is the most common battery chemistry for EVs. Thus, the controller can be switched between three alternatives, i.e., constant power (CP), CC, and CV, depending on the desired mode of operation. The output for all control modes is the duty ratio of the buck switch SW_5 .

III. AVERAGE MODELING

In the analysis of the impact of bidirectional chargers on the LV distribution system, a number of these chargers need to be considered. Hence, using a detailed model of the bidirectional charger could require a significant amount of computational time, because of the high switching frequency. Hence, an average model of the charger is developed in this section to be used in LV distribution system integration studies, as demonstrated in Section V. This model can also be used to derive a small signal average model and obtain a transfer function, which is useful in design and tuning of the control strategy of the smart charger.

The following switching functions can be defined for the two legs of the full-bridge ac/dc converter of Fig. 1:

$$SF_1 = \begin{cases} 1 \rightarrow SW_1 : ON, SW_2 : OFF \\ 0 \rightarrow SW_1 : OFF, SW_2 : ON \end{cases} \quad (2)$$

$$SF_2 = \begin{cases} 1 \rightarrow SW_3 : ON, SW_4 : OFF \\ 0 \rightarrow SW_3 : OFF, SW_4 : ON \end{cases} \quad (3)$$

One can write v_c and i_s in terms of SF_1 and SF_2 as follows:

$$v_c = (SF_1 - SF_2)v_{dc} \quad (4)$$

$$i_{dc} = (SF_1 - SF_2)i_s \quad (5)$$

In average modeling, SF_1 and SF_2 can be replaced by their low-frequency components, as follows:

$$SF_1 \approx 0.5 + 0.5m_1 \quad (6)$$

$$SF_2 \approx 0.5 + 0.5m_2 \quad (7)$$

where m_1 and m_2 are the modulation signals (normalized to the peak value of the triangular carrier signal) used to control the switches, represented as:

$$m_1 = M \cos(\omega t + \theta) = v_{mod} \quad (8)$$

$$m_2 = -M \cos(\omega t + \theta) = -v_{mod} \quad (9)$$

where M is the modulation index that is allowed to vary between 0 and 1 in the linear range of PWM. Therefore, from (4) to (9), and excluding the high-frequency contents, v_c and i_{dc} can be written in the following form:

$$v_c = 0.5(m_1 - m_2)v_{dc} = v_{mod}v_{dc} \quad (10)$$

$$i_{dc} = 0.5(m_1 - m_2)i_s = v_{mod}i_s \quad (11)$$

Assuming complementary switch control signals for SW_5 and SW_6 , two topological modes can be identified for the bidirectional buck-boost converter:

- Topological mode 1: In this case, SW_5 is ON and SW_6 is OFF, resulting in:

$$\frac{di_{L_f}}{dt} = \frac{1}{L_f}v_{dc} - \frac{1}{L_f}v_b \quad (12)$$

$$\frac{dv_{dc}}{dt} = \frac{1}{C_{dc}}i_{dc} - \frac{1}{C_{dc}}i_{L_f} \quad (13)$$

$$\frac{dv_b}{dt} = \frac{1}{C_f}i_{L_f} - \frac{1}{C_f}i_b \quad (14)$$

- Topological mode 2: Here, SW_5 is OFF and SW_6 is ON, yielding:

$$\frac{di_{L_f}}{dt} = -\frac{1}{L_f}v_b \quad (15)$$

$$\frac{dv_{dc}}{dt} = \frac{1}{C_{dc}}i_{dc} \quad (16)$$

$$\frac{dv_b}{dt} = \frac{1}{C_f}i_{L_f} - \frac{1}{C_f}i_b \quad (17)$$

Averaging the first-order differential equations (12)-(17) over a switching period, one can obtain the following expressions, where D_{SW_5} is the duty cycle for SW_5 in Fig. 1:

$$\begin{aligned} \left. \frac{di_{L_f}}{dt} \right|_{av} &= D_{SW_5} \left(\frac{1}{L_f}v_{dc} - \frac{1}{L_f}v_b \right) \\ &\quad + (1 - D_{SW_5}) \left(-\frac{1}{L_f}v_b \right) \\ &= D_{SW_5} \frac{v_{dc}}{L_f} - \frac{v_b}{L_f} \end{aligned} \quad (18)$$

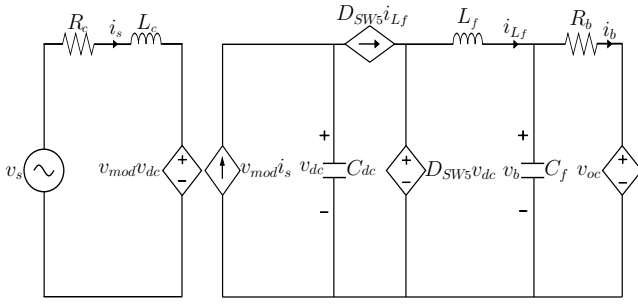


Fig. 4. Average model of bidirectional charger.

$$\begin{aligned} \left. \frac{dv_{dc}}{dt} \right|_{av} &= D_{SW_5} \left(\frac{1}{C_{dc}} i_{dc} - \frac{1}{C_{dc}} i_{L_f} \right) \\ &\quad + (1 - D_{SW_5}) \left(\frac{1}{C_{dc}} i_{dc} \right) \\ &= \frac{1}{C_{dc}} i_{dc} - D_{SW_5} \frac{i_{L_f}}{C_{dc}} \end{aligned} \quad (19)$$

$$\left. \frac{dv_b}{dt} \right|_{av} = \frac{1}{C_f} i_{L_f} - \frac{1}{C_f} i_b \quad (20)$$

From these average expressions, the equivalent circuit of Fig. 4 can be derived. Note that this model does not account for converter losses to keep it simple, since considering them implies modeling the non-idealities of switches, diodes, capacitors and inductors, which is needed if the efficiency of the converter is under investigation, which is not the case here, as the model concentrates on properly representing the dynamic response of the developed smart charger. The losses can be readily approximated by adding resistances to the controllable voltage and current sources that represent converter switches in the model. Moreover, the battery is modeled as a Thevenin equivalent, with v_{oc} and R_b being functions of SoC and i_b .

The main purpose of the model is to speed-up time domain simulations involving several chargers in a distribution grid. The model is mainly intended to capture low-frequency dynamics, neglecting the switching frequency dynamics, which are very small due to filtering, and thus allowing to determine set points for smart charging in LV networks, which is the main application of the proposed model. The model also allows to design the smart charger controller, as it captures the main relevant dynamics for that purpose. Furthermore, it allows studying the effects on batteries of the smart charger, which will not be possible with a simpler model with a controllable load and source.

The proposed model is designed to be integrated in mathematical models of the LV distribution system network to calculate control settings of the actual smart charger. These settings are obtained here based on a heuristic approach to avoid overloading of the distribution system transformer and improve voltage profiles in the LV network, thus becoming an integral part of smart charging strategies in distribution feeders, as explained and demonstrated in detail in Section V.

IV. VALIDATION OF AVERAGE MODEL

In this section, the charger's average model developed in Section III is verified against a prototype of a Level 1, 1.92 kVA/120 V bidirectional charger built in the lab (see Fig. 5) [31]. The prototype receives control signals through a Wi-Fi link, which allows an external agent, such as an aggregator or distribution system operator, to remotely control the charging or discharging of the EV battery. The main components of the prototype are:

- 1) The power converter, which implements the topology described in subsection II-A, with the parameter values given in Table I.
- 2) The control board, which interconnects all voltage and current transducers, gate drive modules and the central control unit (CCU), that in this prototype is a TMS320F2808 DSP, and is mainly in charge of performing the control strategies described in subsections II-B and II-C, using the parameters depicted in Tables I and II. These parameters were selected following the typical design procedure found in the technical literature for full-bridge and bidirectional buck-boost converters [32], with the exception of the dc-link capacitor, which is dimensioned considering that the converter is also used as a reactive power source, as per the method described in [7].
- 3) The lithium-ion battery model GBS-LFMP40AH from Elite Power Solutions (4.1 kWh, 102.4 V) and the corresponding battery management system.
- 4) The communications controller, which enables the remote control of the charger using a web page that was implemented using the SN8200 EVK Wi-Fi module from Murata. Wi-Fi technology was chosen because most of the current home energy management systems (e.g., Peaksaver Plus systems in Ontario [33]) are being designed to communicate with the user and utilities through Wi-Fi interfaces and the Internet. Thus, the chosen Wi-Fi controller broadcast a web page with a user interface to select the mode of operation of the charger (CC-CV or smart charging), so that P and Q set points can be defined in smart-charging mode. This web interface also provides operational information such as dc-link voltage, ac voltage, ac current, P, Q, battery SoC and status messages, which is useful for measuring and monitoring purposes.

To compare the performance of the average model with that of the prototype, a charger with the same characteristics of the prototype was simulated in the PSCADTM environment [34], using the average model. The charger parameters used in the simulation were the same as those of the prototype, as per Tables I and II. The average model simulation was performed using a 50 μs time step, which was defined through trial and error as an appropriate value to capture all the variations in voltage and current signals. It is important to mention that if a switching model was used, a 50 μs time step would be insufficient to capture the dynamics of the 20 kHz PWM signal.

A. Steady-state Response

To compare the steady-state response of the average model in the four quadrants of the P-Q plane, as well as on the boundaries of the quadrants, the simulation and experimental results are presented in Fig. 6. These plots demonstrate that the charger is capable of four-quadrant operation, with the average model being able to represent the operation with high accuracy. Purely reactive requests are also demonstrated, where the current lags or leads the voltage by 90° . Observe that the steady-state current and voltage signals from the average model and the prototype are very similar for all analyzed P-Q plane operating points.

The prototype signals contain some noise, and in several cases a third harmonic can be observed in current signals, signified by flattening of current signal around zero-crossing points. This current harmonic can appear in a full-bridge ac/dc converter when the dc-link voltage measurement signal is passed to the control loop without appropriate filtering of the second harmonic ripple [35]; potential solutions to this include improving the filtering of input control signals, increasing the size of the coupling inductor, and retuning the PI regulators in the ac/dc converter. There were also issues producing a stable current wave shape which is a result of poor current tracking. This is in part a result of the chosen current sensor, and the ac current conditioning circuit linking the measured current to the analog-to-digital converter (ADC) on the CCU.

B. Dynamic Response

A comparison between the dynamic behavior of the prototype and the average model was also performed. For this purpose, the step response for V_s , I_s , P_s , Q_s , V_b , V_{dc} , and I_b in two transitions were captured. The first transition was from 1.1 kW and 0 kVAR to -1.1 kW and 0 kVAR, and the second transition was from -1.1 kW and 0 kVAR to 1.1 kW and 1.1 kVAR. The results of these scenarios are presented in Fig. 7. Note that the dynamic response of the average model for V_s , I_s , P_s , Q_s , V_{dc} , I_b and V_b follows very closely the corresponding prototype signals. However, observe that V_{dc} on the prototype presents larger overshoots during the transition of P and Q references, and that battery voltage values are not in close agreement. These differences can be attributed to the battery model, which only considers a voltage source behind a resistor, and does not represent the actual dynamic behavior of the battery. To obtain a closer agreement between the result of prototype and those of the average model, a dynamic model of the battery should be used. Additionally, it can be observed that the controller has a slow response, as intended. Since there is no inherent advantage to having a fast time response, which can lead to overshoot, potentially charging the battery beyond the limit it is rated for, the dc filter values were chosen such that it would not only filter the ripple in the P-Q requests, but also slow the response down and eliminate overshoot. The response time of the active power controller is much shorter than that of the reactive power controller, since the active power controller is directly coupled to the battery current.

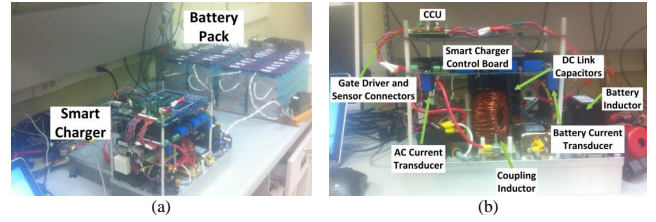


Fig. 5. Bidirectional charger prototype (a) smart charger-battery pack layout, and (b) smart charger side view [31].

TABLE I
SYSTEM PARAMETERS

Description	Parameter	Value	Unit
Smart Charger VA Rating	S	1.92	kVA
Absolute Maximum Reactive Power	Q_s	1.92	kVAR
Absolute Maximum Active Power	P_s	1.92	kW
Grid Voltage	V_s	120	V
Maximum AC Current	I_s	16	A
Absolute Maximum Battery Current	I_b	20	A
Nominal Open Circuit Battery Voltage	V_{oc}	105	V
DC Link Voltage	V_{dc}	280	V
Coupling Inductor	L_C	1.65	mH
DC Link Capacitor	C_{dc}	2	mF
DC/DC Filter Inductor	L_f	1.5	mH
DC/DC Filter Capacitor	C_f	1	mF
Switching Frequency	f_s	20	kHz

TABLE II
CONTROLLER PARAMETERS

PI controller	(1)	(2)	(3)	(4)	(5)	(6)	(7)	(8)
k_i	2.5	160	5	80	0.5	1	1	1
k_p	0.25	15	0.07	10	0.1	0.001	0.001	0.001

V. LOW-VOLTAGE DISTRIBUTION SYSTEM EV INTEGRATION

A. Results

The average model of the bidirectional charger was used to simulate a typical secondary distribution system composed of 10 residential loads, fed from a 50 kVA, 12.47 kV/240 V-120 V single-phase transformer (see Fig. 8), and 10 EVs that were connected to each residential load. The specifications of the secondary distribution system correspond to the residential CIGRE benchmark of a North-American secondary distribution system presented in [36]. Residential loads were assumed to be evenly distributed between the split secondary system phases, and follow the demand curves and power factors specified in the CIGRE benchmark. It was assumed that each residential load had an EV with a single-phase charger, according to the specifications of the prototype introduced in Section IV, i.e., 1.92 kVA/120 V, and a 16 kWh battery. The simulations were implemented using the PSCADTM software [34].

A three-winding transformer model was used for the distribution transformer, and a coupled wire model was used for service cables. Residential loads were modeled as constant-impedance loads, with the impedances determined by the given power in a time interval and the nominal voltage. The bidirectional chargers and their average models were implemented using controlled voltage and current sources available in the PSCADTM library. The controllers described in Section II were implemented using the parameters of Tables I and II.

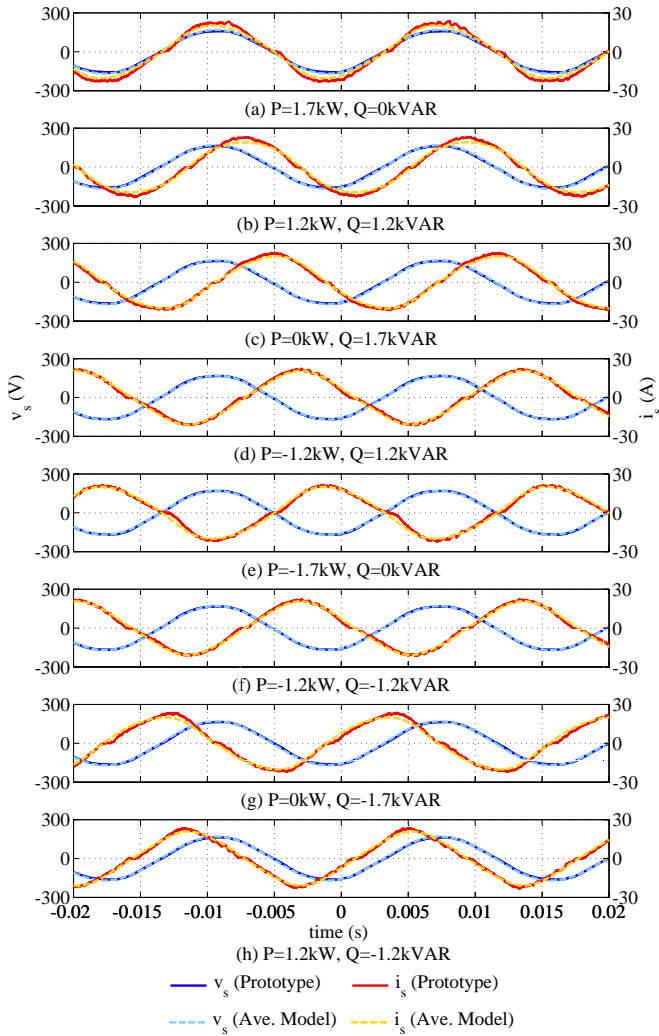


Fig. 6. Steady-state responses for different PQ requests.

For all case studies, the simulation time was 288 s, and the simulation step was $50 \mu\text{s}$, representing an advantage in terms of simulation time steps and simulation times when compared to using a complete model considering the switching effects, which requires much smaller simulation steps. Each second in the simulation represents the loading conditions in a 5 minute interval; thus, the power references for the residential loads are adjusted each second, and active and reactive power references for bidirectional chargers are adjusted depending on the type of control, as explained next.

Three case studies were implemented to analyze the impact of EV charging and different V2G strategies on the residential system. All cases simulate CC-CV charging, assuming that all EVs start charging at 1:00 am with 20% state of charge (SoC), until reaching 85% SoC. The battery voltage for all EVs is calculated using the expressions $V_{oc} = 2.9132SoC + 104.08$ for charging, and $V_{oc} = 3.5862SoC + 103.26$ for discharging, which approximate the voltage of the battery pack used in the prototype. R_b is assumed to be 0.0625Ω for charging, and 0.05625Ω for discharging. CC charging is switched to CV charging when the battery reaches an SoC of 75%.

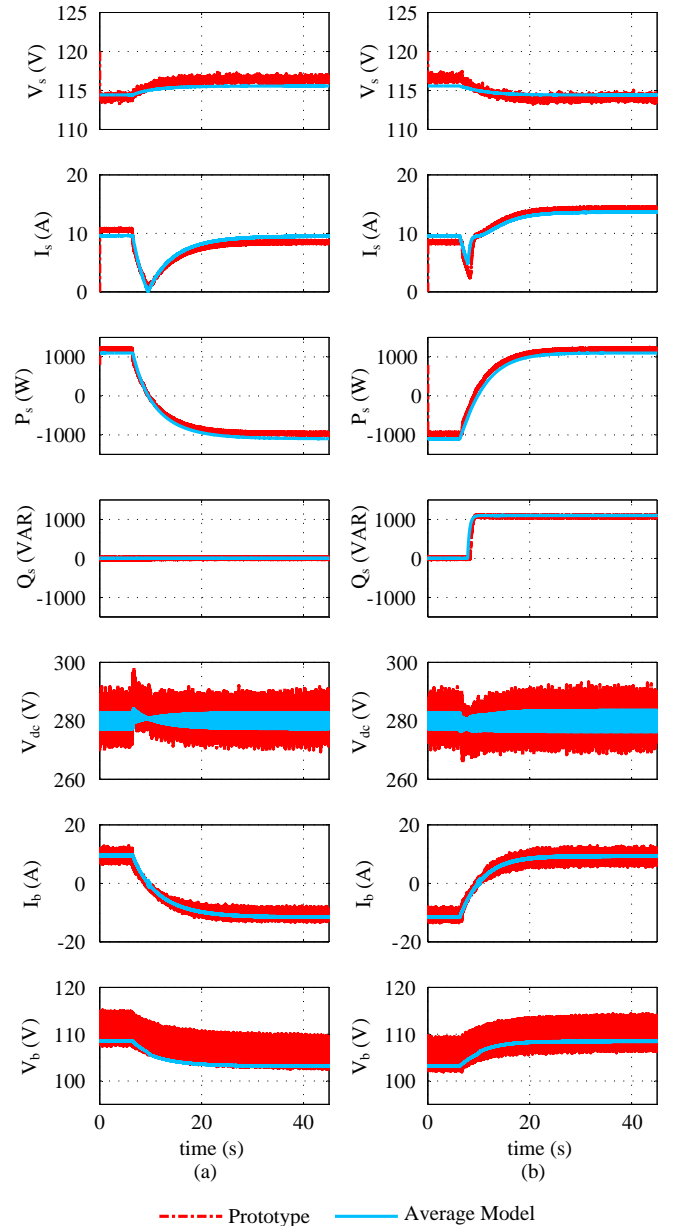


Fig. 7. Step response (a) from $P=1.1\text{kW}$ and $Q=0 \text{ kVAR}$ to $P=-1.1 \text{ kW}$ and $Q=0 \text{ kVAR}$, and (b) from $P=-1.1\text{kW}$ and $Q=0 \text{ kVAR}$ to $P=1.1 \text{ kW}$ and $Q=1.1 \text{ kVAR}$.

The V2G strategies are assumed to be applied following the afternoon commuting, and EVs are divided in the following three sets to study the effect of different arriving times: Set 1 is composed of EVs at nodes R_5 , R_9 , R_{12} , and R_{13} , following the CIGRE benchmark notation, arriving at 6:00 pm; Set 2 is composed of EVs in nodes R_6 , R_8 , and R_{11} , arriving at 7:00 pm; and Set 3 is composed of EVs at nodes R_7 , R_{10} , and R_{14} , arriving at 8:00 pm.

The first case study presents a Q compensation control by an external agent. It is assumed that this external agent is a controller located at the distribution transformer, receiving real-time measurements of reactive power consumption of the residential network. Thus, the controller determines Q compensation requirements of the residential distribution system,

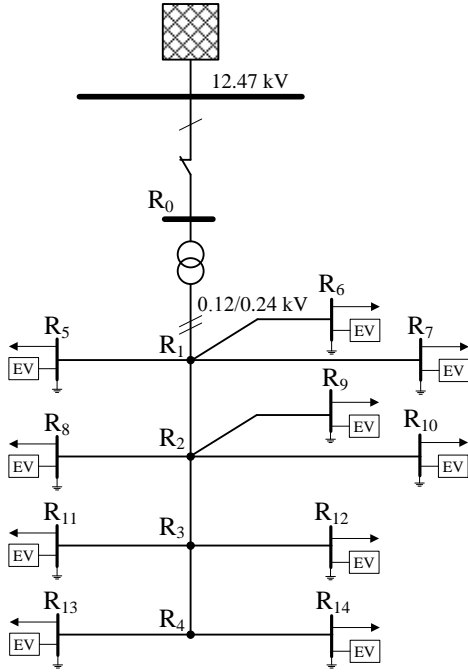


Fig. 8. Secondary distribution system model.

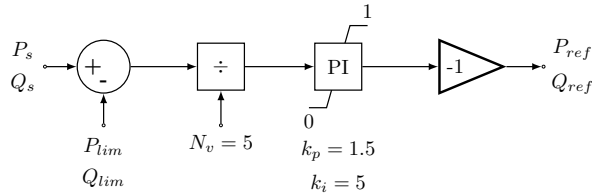


Fig. 9. P and Q compensation control.

and determines the Q references for all EV chargers that are connected to the grid, as depicted in Fig. 9, where Q_{lim} for this controller is assumed fixed at 4 kVAR, and the maximum available Q per charger is assumed to be 1 kVAR.

The second case study presents a voltage droop function which is implemented locally in all bidirectional chargers, as proposed in [37] for the case of solar panel applications. The droop function

$$Q_{EV} = \begin{cases} 1 & V > 1.03pu \\ \frac{100}{3}(V - 1) & 0.97pu \leq V \leq 1.03pu \\ -1 & V < 0.97pu \end{cases} \quad (21)$$

determines a reactive power reference as a function of the charger local voltage. Hence, the reactive power compensation depends on the connection point, since this value is related to local voltage.

The third case study is referred to as P compensation and is identical to the first case, except that it is used for active power. In this case, P_{lim} for the control strategy of Fig. 9 is assumed fixed at 36 kW, and the maximum available P per charger is assumed to be 1 kW.

Figure 10 presents the results for active and reactive power at the distribution transformer. For the three cases, a new peak appears during the early morning due to simultaneous charging

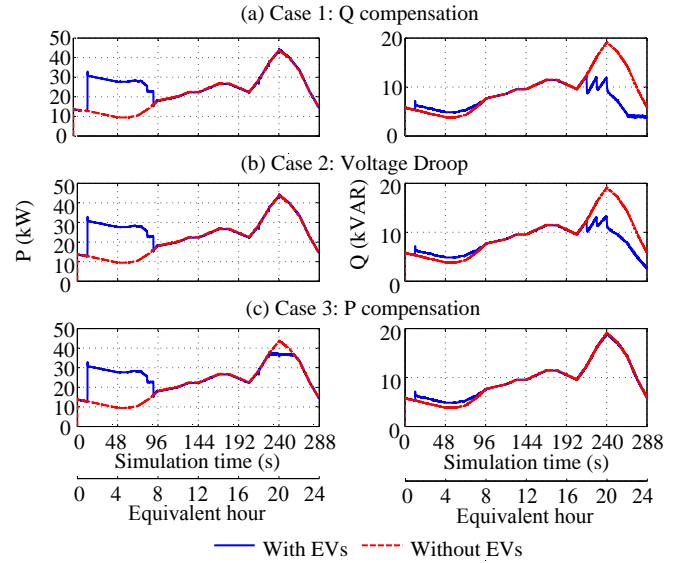


Fig. 10. Active and reactive power at distribution transformer.

of EVs; however, this peak does not surpass the normal evening peak. Q compensation and voltage droop operate by decreasing the reactive power consumption during the peak hours and are able to slightly improve the voltage profile, as seen in Fig. 11(a) and (b), compared to the voltage at the last node (R_{14}) without EVs. The Q compensation strategy is able to inject more reactive power, since it follows the actual reactive power consumption; however, before 10 pm, the need for reactive power surpasses the capacity of EV chargers, as it can be seen in Fig. 12(a). From Fig. 12(b), it is evident that the chargers do not reach their reactive power limit when operating in voltage droop control. Note that Figs. 10, 11, and 12 contain two scales, i.e., the actual simulation time and the corresponding equivalent real-time scale. The first scale corresponds to a simulation time of 288 s, while the second corresponds to 24-hours, so that 1 second of simulation time represents 5 minutes of real time.

P compensation shaves the active power curve at 36 kW during the peak period, according to the fixed limit set for the P of each charger, as seen in Fig. 10(c). This has an effect on the voltage profile (see Fig. 11(c)), which is also improved thanks to less current coming from the distribution transformer. As seen in Fig. 12(c), the chargers inject P when needed after the vehicles arrive, without reaching the limit of 1 kW. Note that Figs. 10, 11 and 12 show transients at certain points, which are due to the dynamic response of the average models following a change in reference signals. As seen in Fig. 3, the charger is able to change the mode of operation between CC, CV and CP. When the charger connects, the control is switched to CP mode, and the duty cycle changes its value as per the PI controller; hence, the transients that are seen in the graph for active power are due to the transitions in the mode of operation and set points. To illustrate the actual duration of these transients, a 300 s simulation was carried out for a 5-minute window in which the EV chargers switch from CV to CP modes at $t=150$ s. The simulation took 1 hour and 2

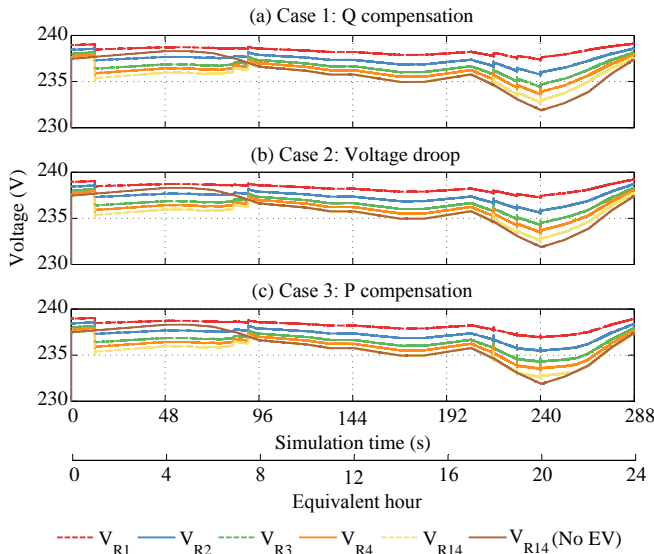


Fig. 11. Voltage at different nodes of the secondary distribution system.

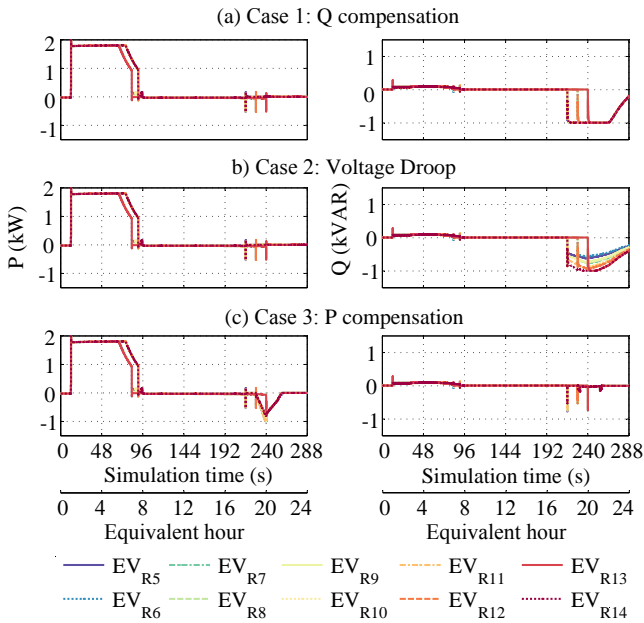


Fig. 12. Active and reactive power at EV chargers.

minutes to complete running in a 1.87 GHz Intel Xeon CPU, which would result in about 13 days of simulation time to complete a full 24-hour period in this time scale; this is the reason why the simulations shown in Figs. 10-12 are carried out using a faster time scale than real-time. The results of this simulation are presented in Fig. 13; observe that in Fig. 13(a) the transient appears as an instantaneous transient when in reality it has a duration of almost 0.5 s, as seen in Fig. 13(b). In practical implementations, these transients have to be minimized in order to avoid harmful effects on charger switches and EV batteries.

A fourth case study is carried out to analyze possible dynamic interactions of bidirectional EV chargers in LV distribution networks, considering set-point changes to the EV

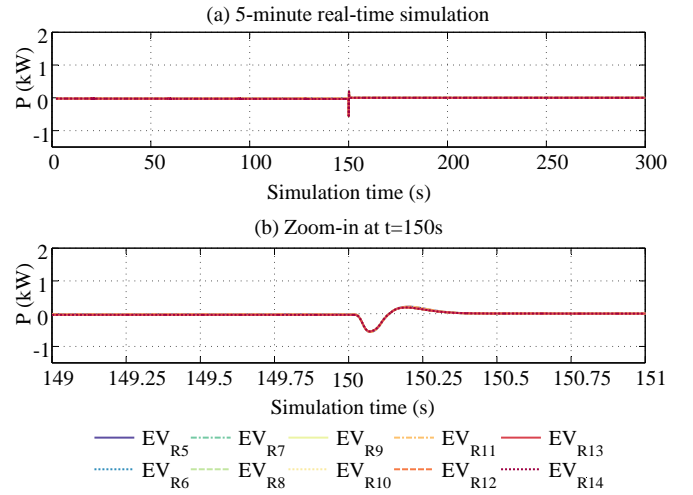


Fig. 13. Control mode transition between CV and CP.

bidirectional chargers in a short period of time. In this case, the residential loads are assumed constant and at their maximum levels, as defined in the CIGRE benchmark. EVs at nodes R₅, R₇, R₉, R₁₁, and R₁₃ are assumed to absorb 1.92 kW each, and EVs at nodes R₆, R₈, R₁₀, R₁₂, and R₁₄ are assumed to operate in voltage droop control mode. It is also assumed that EVs start to operate in pairs every two seconds, following the sequence R₅-R₆, R₇-R₈, R₉-R₁₀, R₁₁-R₁₂, and R₁₃-R₁₄. In this case, the simulation time is 12 s, and the simulation step was 50 μ s.

For the last case study, Fig. 14 shows the details of active and reactive power dynamic transitions in EV chargers, and Fig. 15 depicts the effects of these transitions on the distribution transformer and node voltages, with and without considering the operation of EVs in voltage droop mode. Observe that the active and reactive power for all EVs have a slow transition, as expected from the experiments presented in Section IV, slowly and slightly increasing the total active power at the distribution transformer. The transients observed in Fig. 12, which appear as a consequence of the dynamic response of the EV charger controller, also appear in Fig. 14, and have only a small effect on the node voltages and transformer active and reactive power, as observed in Fig. 15. Note that the voltages improve following the dynamics of the droop controller and the charger.

B. Discussion

Options for controlling voltage profiles in LV networks are very limited; thus, the presented case studies demonstrated three control options that can be accomplished with bidirectional EV smart chargers to help with this task. The results show that P compensation strategy is better to boost the voltage in LV residential networks, since power factor tends to be high in residential loads. However, the main advantage of the proposed injection of reactive power from the smart charger is that it does not discharge the battery (except to compensate for the ac/dc converter losses), since this can be accomplished with the dc link capacitor. These types of chargers could also

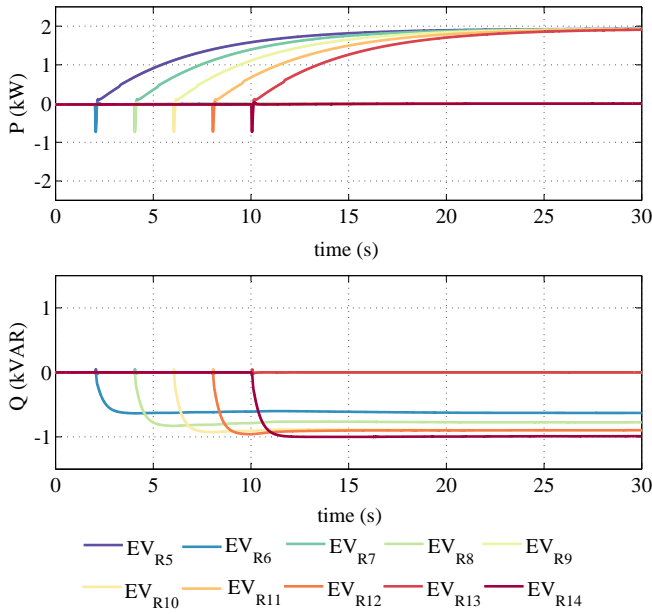


Fig. 14. Active and reactive power for EVs in Case 4.

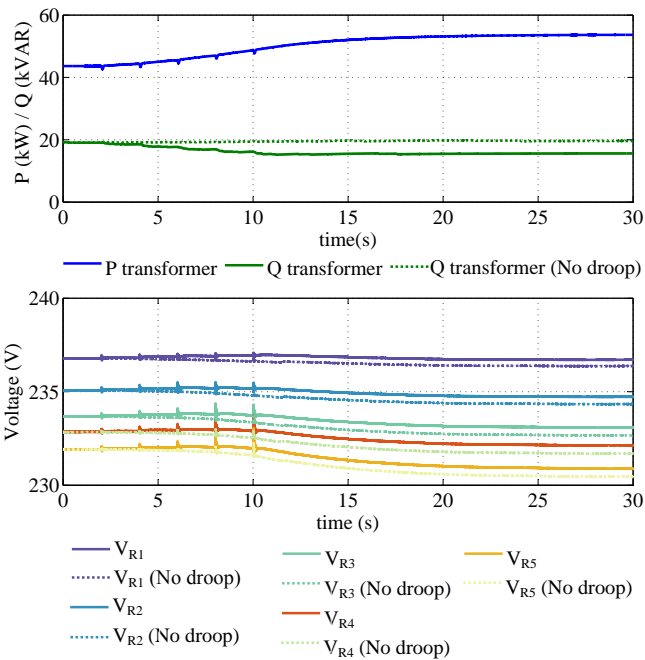


Fig. 15. Active and reactive power at distribution transformer and node voltages in Case 4.

be used as an aggregated reactive power source to control the voltage profile at the medium voltage level, acting as a controllable distribution feeder capacitor, which is an approach the authors are currently studying.

The most important challenge for the integration of four-quadrant bidirectional chargers in actual distribution systems is the adequate control of P and Q to mainly charge the battery while supporting the distribution grid. This task can be complex, because P and Q are coupled and the chargers are normally located on-board the vehicles, and thus the chargers are connected to the grid for only a limited time. Since

the reactive power capability of the charger only depends on the full-bridge ac/dc converter, a practical implementation approach of the proposed smart charging scheme to facilitate control and provide more reliable services to the grid would be to split the converter, thus integrating the Stage 1 into the EV connection box, and keeping the Stage 2 on-board the vehicle. This would require changing the ac EV charging interface to dc, which could fit very well with fast charging standards.

VI. CONCLUSION

This paper presented the prototype and an average model of a single-phase, two-stage, Level 1 bidirectional smart charger composed of a full bridge ac/dc converter and a bidirectional buck-boost converter. The ac/dc converter used a dq frame controller with an additional loop to control reactive power, and the dc/dc converter employed a PI controller with an additional loop to control active power, thus giving the charger the capability of independent P and Q control. The average model was validated using measurements from an actual smart charger prototype, verifying its steady-state response in all four quadrants of the P-Q plane, as well as the step response when P and Q references are changed. The results obtained from the average model were shown to be generally in close agreement with those of the prototype, although some improvements can be made by including a dynamic model for the battery. Finally, the average model was used in the integration study of the smart charger prototype in a residential distribution system for three V2G strategies. The model proved to be appropriate for representing the steady-state response and cycle-to-cycle dynamics of the chargers when interacting with a distribution system. The proposed model will be used to design smart charging and discharging strategies and analyze their impacts on distribution feeders.

REFERENCES

- [1] J. A. P. Lopes, F. J. Soares, and P. M. R. Almeida, "Integration of electric vehicles in the electric power system," *Proc. IEEE*, vol. 99, no. 1, pp. 168–183, 2011.
- [2] W. Kempton and J. Tomić, "Vehicle-to-grid power fundamentals: Calculating capacity and net revenue," *Journal of Power Sources*, vol. 144, no. 1, pp. 268–279, 2005.
- [3] "Power to spare - Nissan and Endesa sign pledge to promote Europe's first mass market vehicle to grid system," Nissan, 2015. [Online]. Available: <http://newsroom.nissan-europe.com/EU/en-gb/Media/Media.aspx?mediaid=130188>
- [4] B.-R. Lin, D.-J. Chen, and H.-R. Tsay, "Bi-directional ac/dc converter based on neutral point clamped," in *Proc. IEEE International Symposium on Industrial Electronics (ISIE)*, vol. 1, 2001, pp. 619–624.
- [5] B. Lin, T. Hung, and C. Huang, "Bi-directional single-phase half-bridge rectifier for power quality compensation," *IEE Proceedings-Electric Power Applications*, vol. 150, no. 4, pp. 397–406, 2003.
- [6] X. Zhou, G. Wang, S. Lukic, S. Bhattacharya, and A. Huang, "Multi-function bi-directional battery charger for plug-in hybrid electric vehicle application," in *Proc. IEEE Energy Conversion Congress and Exposition*, 2009, pp. 3930–3936.
- [7] M. C. Kisacikoglu, "Vehicle-to-grid (V2G) reactive power operation analysis of the EV/PHEV bidirectional battery charger," Ph.D. dissertation, University of Tennessee, Knoxville, 2013.
- [8] T. Tanaka, T. Sekiya, H. Tanaka, M. Okamoto, and E. Hiraki, "Smart charger for electric vehicles with power-quality compensator on single-phase three-wire distribution feeders," *IEEE Trans. Ind. Appl.*, vol. 49, no. 6, pp. 2628–2635, 2013.

- [9] V. Monteiro, J. G. Pinto, B. Exposto, H. Goncalves, J. C. Ferreira, C. Couto, and J. L. Afonso, "Assessment of a battery charger for Electric Vehicles with reactive power control," in *Proc. IECON (Industrial Electronics Conference)*, 2012, pp. 5142–5147.
- [10] M. Kesler, M. C. Kisacikoglu, and L. M. Tolbert, "Vehicle-to-grid reactive power operation using plug-in electric vehicle bidirectional onboard charger," *IEEE Trans. Ind. Electron.*, vol. 61, no. 12, pp. 6778–6784, 2014.
- [11] M. Kisacikoglu, M. Kesler, and L. M. Tolbert, "Single-phase on-board bidirectional PEV charger for V2G reactive power operation," vol. 6, no. 2, pp. 767–775, March 2015.
- [12] O. Sundström and C. Binding, "Flexible charging optimization for electric vehicles considering distribution grid constraints," vol. 3, no. 1, pp. 26–37, 2012.
- [13] I. Sharma, C. Cañizares, and K. Bhattacharya, "Smart charging of PEVs penetrating into residential distribution systems," vol. 5, no. 3, pp. 1196–1209, 2014.
- [14] A. Dubey, S. Santoso, and M. P. Cloud, "Average-value model of electric vehicle chargers," vol. 4, no. 3, pp. 1549–1557, 2013.
- [15] D. Maksimović, A. M. Stanković, V. J. Thottuvelil, and G. C. Verghese, "Modeling and simulation of power electronic converters," *Proc. IEEE*, vol. 89, no. 6, pp. 898–912, 2001.
- [16] R. Zhang, M. Cardinal, P. Szczesny, and M. Dame, "A grid simulator with control of single-phase power converters in dq rotating frame," in *Proc. IEEE 33rd Power Electronics Specialists Conference (PESC)*, vol. 3, 2002, pp. 1431–1436.
- [17] Y. Zhang, Z. Jiang, and X. Yu, "Small-signal modeling and analysis of parallel-connected voltage source inverters," in *Proc. IEEE 6th International Power Electronics and Motion Control Conference*, 2009, pp. 377–383.
- [18] A. Yazdani and R. Iravani, *Voltage-sourced converters in power systems: modeling, control, and applications*. John Wiley & Sons, 2010.
- [19] M. R. Abedi, B.-M. Song, and R.-Y. Kim, "Dynamic performance improvement of bidirectional battery chargers using predictive current control," in *Proc. IEEE Power and Energy Society General Meeting*, 2012, pp. 1–8.
- [20] N. Wong and M. Kazerani, "A review of bidirectional on-board charger topologies for plugin vehicles," in *Proc. IEEE 25th Canadian Conference on Electrical & Computer Engineering (CCECE)*, 2012, pp. 1–6.
- [21] M. C. Kisacikoglu, B. Ozpineci, and L. M. Tolbert, "Examination of a PHEV bidirectional charger system for V2G reactive power compensation," in *Proc. IEEE 25th Applied Power Electronics Conference and Exposition (APEC)*, 2010, pp. 458–465.
- [22] M. Yilmaz and P. Krein, "Review of the impact of vehicle-to-grid technologies on distribution systems and utility interfaces," *IEEE Trans. Power Electron.*, vol. 28, no. 12, pp. 5673–5689, 2013.
- [23] L. Shi, A. Meintz, and M. Ferdowsi, "Single-phase bidirectional ac-dc converters for plug-in hybrid electric vehicle applications," in *Proc. IEEE Vehicle Power and Propulsion Conference (VPPC)*, 2008, pp. 1–5.
- [24] M. P. Kazmierkowski and L. Malesani, "Current control techniques for three-phase voltage-source PWM converters: a survey," *IEEE Trans. Ind. Electron.*, vol. 45, no. 5, pp. 691–703, 1998.
- [25] X. Zhou, S. Lukic, S. Bhattacharya, and A. Huang, "Design and control of grid-connected converter in bi-directional battery charger for plug-in hybrid electric vehicle application," in *Proc. IEEE Vehicle Power and Propulsion Conference (VPPC)*, 2009, pp. 1716–1721.
- [26] N. Wong, K. Zhuge, and M. Kazerani, "A comparative evaluation of control techniques for grid-side ac-dc converter in a two-stage level-two bidirectional battery charger," in *Proc. IEEE Transportation Electrification Conference and Expo (ITEC)*, 2013, pp. 1–5.
- [27] O. Hegazy, J. Van Mierlo, R. Barrero, P. Lataire, N. Omar, and T. Coosemans, "A comparative study of different control strategies of on-board battery chargers for battery electric vehicles," in *Proc. IEEE 8th International Conference and Exhibition on Ecological Vehicles and Renewable Energies (EVER)*, 2013, pp. 1–6.
- [28] M. Gonzalez, V. Cardenas, and F. Pazos, "DQ transformation development for single-phase systems to compensate harmonic distortion and reactive power," in *Proc. 9th IEEE International Power Electronics Congress*, 2004, pp. 177–182.
- [29] N. N.-Y. Wong, "Design of a Two-Stage Level-Two Bidirectional On-Board Battery Charger for Plugin Vehicles," Master's thesis, University of Waterloo, 2013.
- [30] U. Miranda, L. Rolim, and M. Aredes, "A dq synchronous reference frame current control for single-phase converters," in *Proc. IEEE 36th Power Electronics Specialists Conference (PESC)*, 2005, pp. 1377–1381.
- [31] J. Morris, "Design and Testing of a Bidirectional Smart Charger Prototype," Master's thesis, University of Waterloo, 2015.
- [32] N. Mohan and T. M. Undeland, *Power electronics: converters, applications, and design*. John Wiley & Sons, 2007.
- [33] "Peaksaver plus®," Hydro One Inc., 2015. [Online]. Available: <http://www.hydroone.com/MyHome/SaveEnergy/Pages/Peaksaver.aspx>
- [34] "Users guide on the use of PSCAD v4.3.1," Manitoba-HVDC Research Center, p. 492, 2010. [Online]. Available: https://hvdc.ca/uploads/ck/files/reference_material/PSCAD_User_Guide_v4_3_1.pdf
- [35] J. R. Rodríguez, J. W. Dixon, J. R. Espinoza, J. Pontt, and P. Lezana, "PWM regenerative rectifiers: state of the art," *IEEE Trans. Ind. Electron.*, vol. 52, no. 1, pp. 5–22, 2005.
- [36] K. Strunz *et al.*, "Benchmark systems for network integration of renewable and distributed energy resources," Tech. Rep. CIGRE Task Force C.04.02, 2013.
- [37] K. Turitsyn, P. Sulc, S. Backhaus, and M. Chertkov, "Options for control of reactive power by distributed photovoltaic generators," *Proc. IEEE*, vol. 99, no. 6, pp. 1063–1073, 2011.

Mauricio Restrepo (S'13) received the electrical engineer degree and a specialization degree in transmission and distribution systems from Universidad Pontificia Bolivariana, Medellín, Colombia, in 2006 and 2010. He is currently working toward the Ph.D. degree in Electrical and Computer Engineering at the University of Waterloo, ON, Canada. His research interests include electric mobility, simulation and optimization of power systems.

Jordan Morris received the B.A.Sc degree and the M.A.Sc degree in electrical engineering from the University of Waterloo, ON, Canada, in 2012 and 2014. He is currently a Hardware Test Engineer at Tesla Motors.

Mehrdad Kazerani (S'88-M'96-SM'02) received the B.Sc. degree from Shiraz University, Iran, the M.Eng. degree from Concordia University, Canada, and the Ph.D. degree from McGill University, Canada, in 1980, 1990, and 1995, respectively. From 1982 to 1987, he was with the Energy Ministry of Iran. He is currently a Professor at the Department of Electrical and Computer Engineering, University of Waterloo, Waterloo, ON, Canada. His research interests include power electronic circuits and systems design, power quality/active power filters, matrix converters, distributed power generation, utility interface of alternative energy sources, battery electric, hybrid electric and fuel cell vehicles, and FACTS. Dr. Kazerani is a Registered Professional Engineer in the province of Ontario.

Claudio A. Cañizares (S'85-M'91-SM'00-F'07) received the Diploma degree in electrical engineering from Escuela Politecnica Nacional, Quito, Ecuador, and the M.S. and Ph.D. degrees in electrical engineering from the University of Wisconsin/Madison, Madison, WI, USA, in 1984, 1988, and 1991, respectively. He has held various academic and administrative at the University of Waterloo, ON, Canada, since 1993, where he is currently a Full Professor, the Hydro One Endowed Chair, and the Associate Chair of Research in the Department of Electrical and Computer Engineering. His research and consulting work concentrates on stability, control, operating, modeling, simulation, and computational issues in sustainable power and energy systems in the context of competitive markets, smart grids, and microgrids.

Dr. Cañizares was awarded the IEEE Canada Electric Power Medal in 2016, has received several IEEE Power and Energy Society (PES) Working Group Awards, and has held several leadership positions in PES Technical Committees and Subcommittees. He is a Fellow of the Royal Society of Canada and the Canadian Academy of Engineering, and is a Registered Professional Engineer in the province of Ontario.